IN THE WAKE OF BUBBLES:

VELOCITY FIELD MEASUREMENT BY PIV TECHNIQUE

Name: Òscar Conesa Palacios

Title: Master's Thesis

Tutors: Nicolas Dietrich and Pascal Guiraud

Laboratory: LISBP - GPE

University: INSA Toulouse

The content of this scientific article is strictly confidential and belongs to a line of investigation carried out in the LISBP (Laboratoire d'Ingénierie des Systèmes Biologiques et des Procédés) by the team of Transfer-Interphases-Mixtures and under the direction of Nicolas Dietrich, professor associate at INSA Toulouse, Department of Process Engineering and Environment.

IN THE WAKE OF BUBBLES: VELOCITY FIELD MEASUREMENT BY PIV TECHNIQUE

O.CONESA, N.DIETRICH, A.COCKX, P.GUIRAUD

Université de Toulouse INSA, Laboratoire d'Ingénierie des Systèmes Biologiques et des Procédés, INRA-CNRS, 135 avenue de Rangueil, 31077 Toulouse, France.

Keywords: Bubble, Velocity Field, PIV

Abstract

In this paper, the PIV (Particle Image Velocimetry) non-intrusive technique is proposed to calculate the velocity field in the wake of a single bubble rising with a rectilinear path in a quiescent liquid. The aim of this study is to find a general equation which describes the velocity of the flow in a bubble wake. Then, it will be possible to find the term relative to the convective mass transfer around the bubble and, at last, the total mass transfer around it. The set-up tracks the velocity field evolution along the bubble wake for a parallel plane to the bubble path. A spherical bubble is created through a capillary thanks to the constant pressure which applies a syringe pushed by a programmable syringe pump, regulating in this way the advance speed of the injected air. The bubble rises through a glass column containing different solutions, thus presenting different viscosity and Re conditions. Each of these solutions is seeded with silvered tracer particles whose movement allows following the flow velocity field thanks to the PIV method. A high speed camera is located far from the column in order to record the bubble position, size and velocity. This camera is also synchronized with the laser flash by a synchronizer processor. All the experiments have been carried out with bubbles ranging from 0.75 to 3 mm and with 6 hydrodynamic conditions ($1 < Re < 125$).

1. Introduction

The presence of gas-liquid reactors performs vital importance in many engineering processes. The wide range of their applications goes from chemical or biochemical processes to wastewater treatments. Since the efficiency of these reactors is linked to the understanding of the oxygen mass transfer phenomena, it is basic to quantify it in an accurate way in order to achieve mayor efficiency.

Gas-liquid mass transfer process is controlled by two different mechanisms: diffusion and convection. Diffusion is the process which rules in the transport which takes place in the boundary layer, whereas a mix of both diffusion and convection mechanisms is present beyond it. Precisely, it is in the quantification of the convective part of the mass transfer phenomena where the velocity field along the bubble wake plays an essential role. Historically, many techniques have been used in order to calculate flow velocity properties, some of them using venturies tubes, nozzles, rotameters, pitot tubes, calorimetrics etc., thus been quite intrusive. Consequently, flow properties changed and it was not such an easy task to quantify its real state. It became then crucial to find new non intrusive techniques to increase the accuracy of flow properties measurements.

Responding to this necessity, new optical techniques where developed. Their non-intrusive character allowed obtaining mayor precision. Ludwig Prandtl was the first one to use particles to study fluids in a systematic manner. A few years later, the Laser Doppler Velocimetry became widespread for research and industrial use. This method was the predecessor of the current used PIV, the presented method in this paper. This technique allows finding 2D vectors by populating a solution with tracer particles which are supposed to follow ideally fluids motion.

2. Role of a bubble wake velocity field in the bubble wake mass transfer phenomena

As it has been told before, mass transfer phenomena is controlled by both diffusion and convection mechanisms. Nowadays, it is commonly studied through a mass balance on a closed contour delimited by the bubble surface ∂D_B and a geometric contour ∂D_G. In this paper, all the experiments presented have been carried out with single bubbles rising linearly at a velocity U_B. The resulting mass balance applying these conditions is the one that follows:

$$\frac{dm_{O2}}{dt} = \oint_{\partial D_G}\iint \vec{U}_W[O_2].\vec{n}.dS - \oint_{\partial D_B}\iint \vec{J}_{O2}.\vec{n}.dS - \oint_{\partial D_G}\iint \vec{J}_{O2}.\vec{n}.dS \qquad (1)$$

The first term on the right side corresponds to the convective transport, whereas the other ones correspond to diffusion mechanism. Convection effects are expressed by the Reynolds Number ($\mathrm{Re} = \frac{U_B \cdot d_B \cdot \rho}{\mu}$), the bubble shape and the hydrodynamic conditions at the bubble surface. As it can be seen in the balance, it is necessary to quantify the bubble wake velocity field to find this term.

3. PIV technique to find the wake velocity field

3.1 PIV History

In order to calculate the flow velocity field, the chosen method has been the so called PIV (Particle Image Velocimetry). It is a non intrusive technique which allows us to evaluate the instantaneous velocity field as a time function in the flow plane of study. This aptitude to get access to the spatial distribution of the velocity vector makes it, in fact, a complementary technique to those already existents, such as for example LDV (Laser Doppler Velocimetry). This technique was able to obtain all of fluid's velocity measurements at a specific point, whereas PIV produces two dimensional vector fields. The PIV made its appearance in the scientific world around fifteen years ago. Since then, it has been mainly used in two fields: fluid mechanics and processes engineering, in the context of the study of gas, liquid and gas - liquid flows.

3.2 PIV principle

The main principle consists on recording two successive in time images of particles lighted by a laser plane. The local displacement of each of the fluid particles gives us an instantaneous velocity vector.

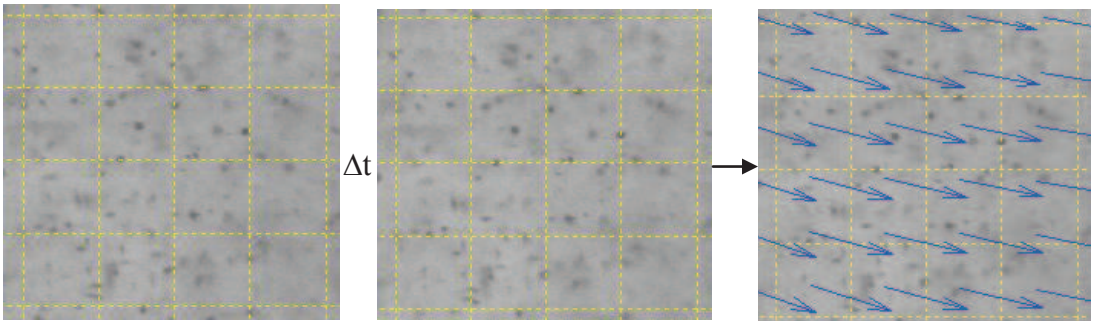

Figure 1. Principle of the Particle Image Velocimetry: Record of two successive in time images

Considering the displacement of all the particles, we can calculate the instantaneous velocity field. In this way, the main base of the PIV method is very simple: the fluid instantaneous velocity is measured by the determination of all the displacements of the tracer particles, which are lighted by a laser plan. The Particle Image Velocimetry is a powerful tool which allows us to find a complete flow map and to validate the simulations. The main condition is that, during the two instants measure, the particle must remain inside the thickness of the lightning plane. Generally, the laser source used is an impulsion laser which delivers two impulsions separated by a time interval Δt (adjustable depending on the velocity you want to measure). Each laser has energy of hundreds of mili joules. All the images are taken by a photo or video camera. Depending on the particles density and the recording type, the images treatment is different.

4. Experimental set-up and procedure

As the goal of this study is to find the bubble wake velocity field**,** there are two basic parameters which have to be known: the bubble velocity U_B and its size d_B.The experimental setup implemented guarantees the obtaining of this information using a PIV system to calculate flow velocity fields and high-speed camera to define the bubble velocity, size and shape. The bubble wake is observed in a plan parallel to the bubble trajectory.

4.1 Experimental set up

The experimental set-up consisted of a transparent column fitted with a bubble injection system and optical equipment which aimed to produce the laser sheet and to obtain bubble rising images. The experimental set-up is depicted in Figure 2. The 100 x 100 x 300 mm^3

column had a square cross-section. Three of its sides were transparent glass and the other one was PMMA. This last one was the one which contained the injection system. The base of the column was made of glass and the top was open. Placed 20mm from the bottom of the column, the injection system was composed of a very thin glass capillary connected to an automatically controlled syringe (Harvard Apparatus PHD 2000). The syringe was filled with oxygen and the flow rate was set to produce only a single bubble at a time. With this requirement, single bubbles were achieved with advance velocities ranging from 10 to $25\frac{\mu m}{\min}$. Bubbles were formed in the middle of the column in solutions containing silver tracer particles. Moreover, a drain tap was fitted at the bottom of the column to evacuate the liquid easily after each series of experiments.

The PIV system was formed by a laser and an image acquisition system provided by Dantec Dynamics. The laser beam was produced by a Nd-YAG laser (15 Hz, Quantel Big Sky – Twins λ_a=532 nm). Its power was of 30 mJ. The laser beam was transformed into a laser sheet thanks to a thin spherical lens. The laser sheet crossed the column vertically along it, in a plane parallel to the bubble ascension.

Each time the laser was used, the cooling level was checked. This level must be 80% of the volume capacity (800 ml). It had to be ensured that the laser plane was fine by adjusting the spherical lenses. The plane had to pass through the plane of rising bubbles and be in the same plane as the camera field of view in order to follow the path correctly.

A CCD (Charge-Coupled-Device) camera (Flowsense 8 bit, Dantec Dynamics, 1600×1186 ppi) allowed registering 8 pairs of photos per second with 256 levels. In addition, an image and synchronizer processor (Flow Map System Hub, Dantec MT) allowed synchronizing the shooting image with the laser flash and the time between two consecutive images too. The PIV images were acquired through specific software (Flow Manager Version 4.60). This program allows calculating the velocity field and other associated parameters, such as:

- The size of the interrogation areas (from 16x16 to 128x128 pixels). A smaller interrogation area demands more time to calculate but the resolution is better.
- The choice of the overlap, which can take values of 0, 25, 50 and 75%. When the value is for example 50%, the tracer particles research zone is expanded in a 50% over the surrounding areas. This fact introduces interdependence and allows following the particles that, initially, go out from the study field.
- The time between two successive images of the camera. This must be such a time that the tracer particles have not moved more than 25% of the study areas.

- The time between two laser pulses. This time is determined by the velocity of the phenomenon.

The tracer particles were silver-coated hollow glass spheres made by Dantec Dynamics. As they did not have to disturb the flow motion, there was no need to introduce a very large quantity. Moreover, at the time of analyzing images and determining the velocity field, there had to be a reasonable number of tracer particles per area of integration with the objective of achieving an acceptable velocity field. This number had to be between 4 and 5. As long it was aimed to obtain the correct velocity field, the tracer particles had to follow the flow perfectly. The seeding had to be uniform and reasonably concentrated in order to follow the flow as well as possible. To achieve this objective, the density was closed to the fluid of study (negligible inertia). If the tracer particles had been too small, it would have come to a relative error due to the Brownian motion (Robert Brown, 1927). The equation (2) establishes a relation between the colloidal diffusion coefficient D_i (relation between the thermal agitation and viscous forces) and the colloidal properties.

$$D_i = \frac{kT}{6\pi\eta r_p} \tag{2}$$

T is the temperature, η the fluid viscosity, r the particle radius and k, Boltzmann's constant. The larger the radius of the particle, the lower importance will have the Brownian motion. The standard deviation of a random displacement of a particle is given by the equation (3).

$$\sigma_p = \Delta x_p \approx \sqrt{2 D_i \delta t} \tag{3}$$

Thus, at 4Hz and a particle diameter of 500 nm, the random displacement was estimated to be 5 microns / s. The minimum flow velocity studied was of the order of several millimeters per second, so it was a non-negligible error rate. We had to therefore focus on larger particles to avoid problems due to Brownian motion. We had to take into account that the bigger the particles were, the bigger was the possibility to fall in sedimentation. Sedimentation velocity of a particle of diameter d is reached when the viscous drag force balances its weight. One obtains the expression (4).

$$V_s = \frac{d_p{}^2 g(\rho_g - \rho_p)}{18\mu} \tag{4}$$

For tracer particles of 100 microns, the sedimentation rate is about 5.45 mm / s, the minimum velocities measured were around a few mm / s. Therefore, the contribution of these two phenomena had to be contained to less than 1% to ensure optimum control. Thus, the optimal size to minimize these two effects was 20 microns.

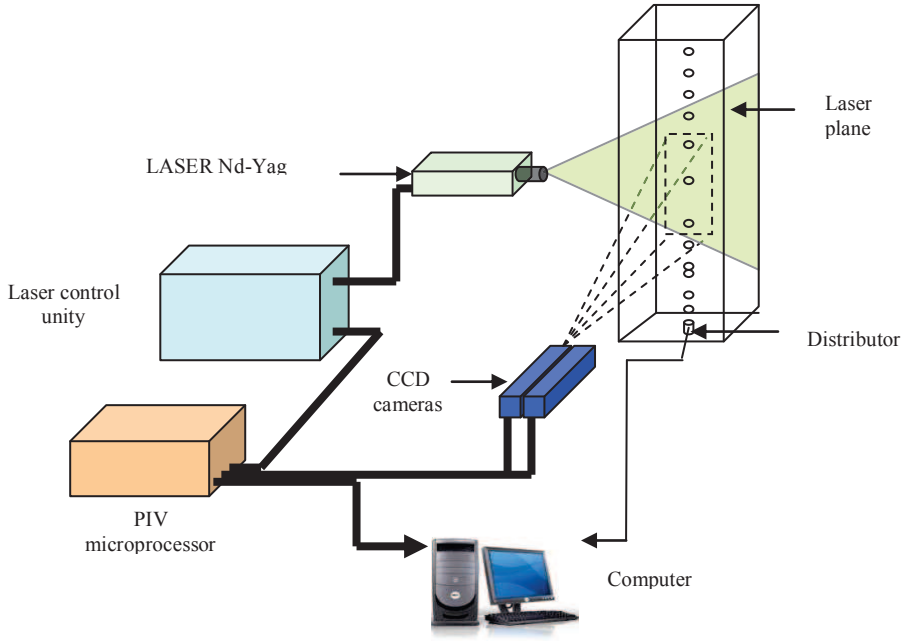

Figure 2. Experimental assembly of the system

4.2 Experimental procedure

For each series of experiments, the firs step was to focus the CCD camera on the laser sheet in presence of the silver tracer particles solution. The second step was to record a set of several images in order to achieve an accurate calibration. Then, the last step was to test and find the best syringe advance velocity conditions aiming to achieve single bubbles ascending with a rectilinear path in the quiescent solution.

4.3 Experimental conditions

The solutions were always populated with silver-coated hollow glass spheres acting as tracer particles. The quantity was not previously fixed, but it had to fulfill two previous conditions: On one hand, the quantity of particles had to be enough so that it allowed obtaining an accurate representation of the velocity field and; on the other hand, the level of turbidity of the solution had to be such that a laser beam was able to get through. Experiments were carried out with 6 different hydrodynamic conditions: three solutions with concentrations of 10, 35 and 50% of glycerol by mass, and three more of 35, 40 and 50 % of HV45 by mass too. All

of them were completed with deionized water. Solution physical properties of water-glycerol solutions were calculated by using the next empirical formulas:

$$Ln[M_{solution}\mu_{solution}(T)] = x_{gly}Ln[M_{gly}\mu_{gly}(T)] + x_{water}Ln[M_{water}\mu_{water}] + x_{gly}x_{water}[B(T) + C(T)x_{gly}] \quad (5)$$

were:

x_{water} and x_{gly} are the molar fractions of water and glycerol in the solution.

$M_{solution}$ is the molar mass of the solution in [gmol^{-1}] defined by the expression $M_{solution} = x_{gly}M_{gly} + x_{water}M_{water}$

$$\mu_{water}(T) = 9.302.10^{-7}\exp[2049.75/T]$$
$$\mu_{gly}(T) = 5.7374.10^{-12}\exp[7681.63/T]$$

μ in Pa.s and T is the temperature in K

$$\upsilon_{solution}(T) = x_{gly}\upsilon_{gly}(T) + x_{water}v_{water}(T) + x_{gly}x_{water}[-2.311 + 1.290x_{gly}]$$
$$\upsilon_{water}(T) = 9.263.10^{-5}T^2 - 4.163.10^{-5}T + 18.011$$
$$\upsilon_{gly}(T) = 3.559.10^{-2} + 72.316$$

υ in cm^3.mol^{-1} and T is the temperature in °C

$$M_{water} = 18.015 g.mol^{-1}$$
$$M_{gly} = 92.095 g.mol^{-1}$$

The bubbles obtained by the injection system were spherical and ascended in a straight line. The bubble diameter was changed by using different sizes of capillary. With regard to bubble velocity, it was given by the physical properties of the solution and by its own size. The velocities reached during the experiments were ranged between 0.125 and 0.285 m/s.

Here is attached a table with all the experimental conditions:

	HV45 50%	***HV45 40%***	***HV45 35%***	***Gly 50%***	***Gly 35%***	***Gly 10%***
Ub (m/s)	0.037	0.069	0.147	0.105	0.209	0.267
d_b (mm)	3	2.9	3	0.8	0.8	0.7
μ (Pa.s)	0.2	0.1	0.05	0.005	0.0025	0.00128
Re	0.552	1.99	8.83	16.7	67	124.6
Cd	32.035	10.888	3.581	2.217	0.689	0.385

5. PIV results

5.1 Bubble diameter; velocity and position

The bubble diameter d_B and velocity U_B by analyzing the shadowgraph images acquired with the CCD camera. The diameter d_B was found by counting the number of millimeters (mm) vertically shadowed by the bubble. The velocity U_B was calculated by comparing the position of the bubble in two consecutive in time images. As the time between 2 images as known (10 ms), the velocity could be easily calculated.

The position (x, y) of the bubble was easily deduced; by counting the number of millimeters (mm) in both axes of each shadowgraph image. In order to face later calculations, the origin (x, y) was set at the centre of the bubble in the first image of its evolution series.

5.2 Bubble wake velocity field obtaining

After each series of measurements, the results were given by the software Flow manager, proportioned by Dantec Dynamics. Consecutive in time images were obtained, allowing getting all the bubbles ascension evolution. From each of these images, it was possible to visualize the vectors velocity field, as well as the obtaining of a data.txt file, which included the information of position (x, y) and velocity (Vx, Vy) for each point of the image. Once all the data of a single bubble evolution was already saved, a matrix was assembled in order to obtain the complete wake velocity field. In this way; coordinate 'x' suffered no changes; whereas coordinate 'y' was recalculated (equation 6), taking into account the temporal offset existent between two consecutive in time images. Finally, for each bubble experiment there was obtained a fourth column matrix (x, y, Vx, Vy).

$$y'_i = y_i + U_B \sum_{i}^{n} t_{i \to i+1} \tag{6}$$

In order to face further calculations, coordinate *y* was finally redefined as coordinate *z*, which represents in fact the same axe (same direction, different sense), but with the new origin set in the middle of the bubble contained in the first image of each bubble ascension series. Once the matrix was already calculated, the next step was to find a tendency in data. With this goal, all the matrix values were represented in a 3D plot by using the mathematical analysis Software Matlab. First analyses revealed a Gaussian tendency in the velocity field (Figure 4).

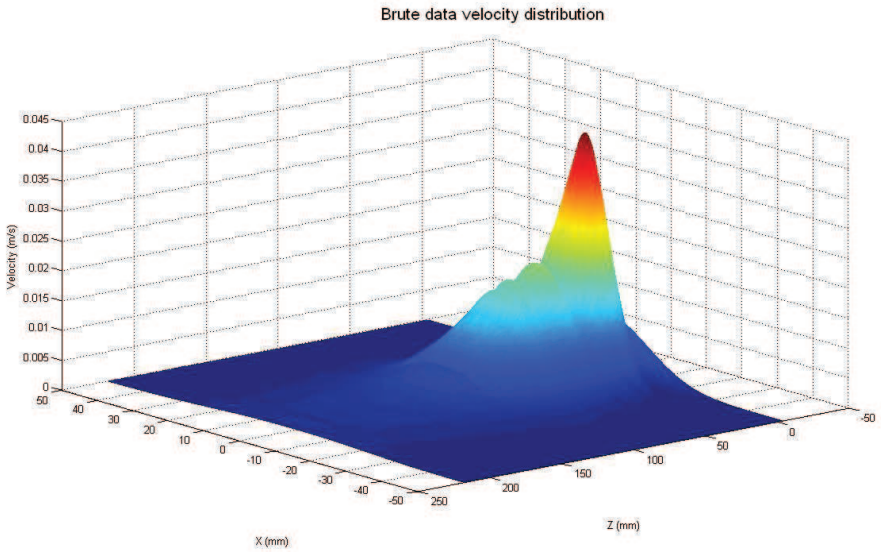

Figure 4. Brute data wake velocity distribution for Re = 2.

It was known then that the velocity field in the bubble wake would follow the next expression:

$$V_W(r,z) = V_{\max}(z).\exp\left(-\left(r^2 / s^2\right)\right) \tag{7}$$

From equation (7), we can see that the velocity field depends on two different parameters for each axe z value: $V_{\max}(z)$ and s .The first one represents the maximum velocity for every wake section along the axe z. It is the highest point in each Gaussian distribution. These maximum values are achieved when radial coordinate r is null. The second term s is relative to the standard deviation of the Gaussian distribution. In this case, this parameter talks about

the width of the Gaussians bell distribution. The next step was then to calculate both $V_{max}(z)$ and s for every bubble wake perpendicular section. This was possible by using the mathematical tool Solver from Microsoft Excel, which uses the simplex method of optimization. Both Gaussian parameters were found by minimizing them values with the real ones obtained experimentally.

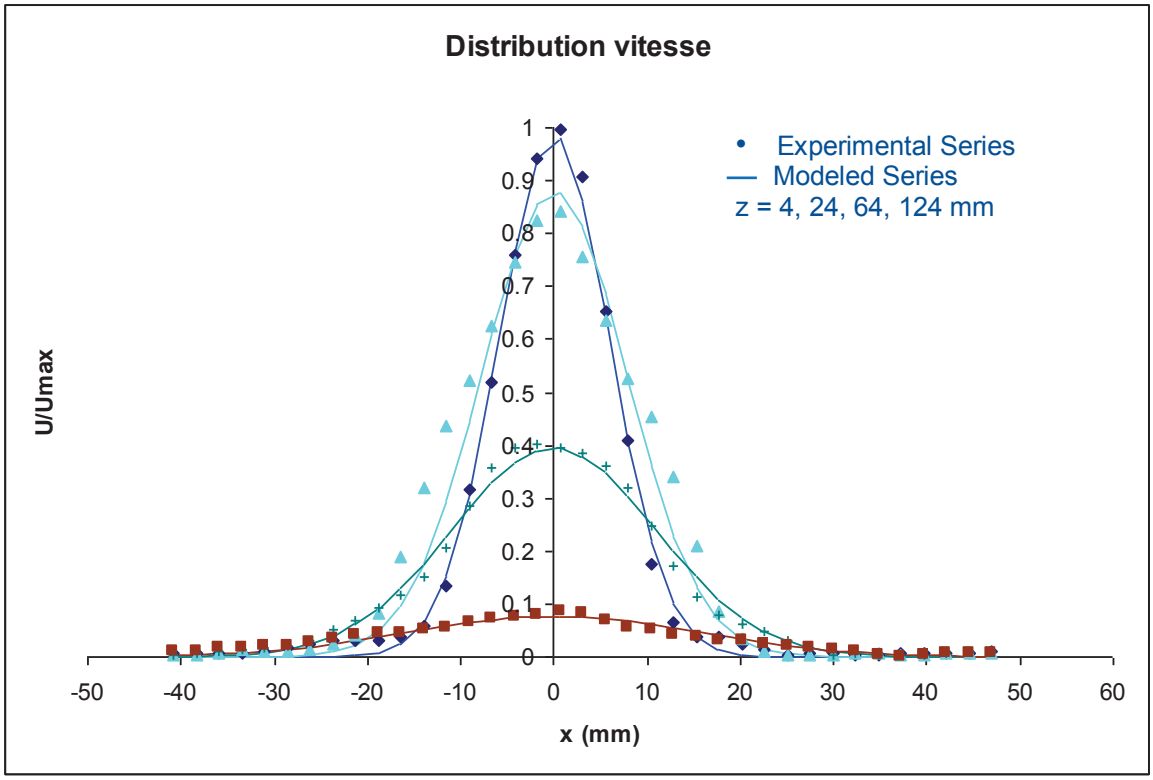

Figure 5. Gaussian normalized velocity distribution for four different sections and Re = 2.

Figure 5 shows an example of different Gaussian distribution along axe z. Dotted series are the ones relative to experimental values, whereas continuous series are the modeled ones. All velocity values have been normalized by dividing each of them by the maximum wake velocity field value.

6. Search of a general equation

Once all the Gaussian Velocity Distributions had been calculated, it was time to search a general equation which described the flow velocity field in the wake of bubble for all bubble sizes and hydrodynamic conditions.

6.1. Models in literature: Oseen's equation

It was done a research process along literature in order to find a theoretical model which described the wake velocity field for a single bubble rising. Finally, it was found the equation proposed by the theoretical physic Carl Wilhelm Oseen (1879, Lund – 1944, Uppsala). Oseen was the director of the Novel Institute for Theorical Physics in Stockholm from 1922 to his death. He is well known by formulating the fundamentals of the *Elasticity theory of liquid crystals*, as well as the *Oseen equations* for viscous fluid flow at small Reynolds numbers. The development of these last equations allowed him to find an asymptotic solution to a body wake velocity field.

The term wake is frequently applied to the entire region of non-zero vorticity on the downstream side of a body in an otherwise uniform stream of fluid. The velocity distribution in the wake velocity field is likely to be quite complicated quite near the body, even if the flow is stagnant. Despite this fact, far downstream the direct effect of the presence of the body is negligible and the streamlines become approximately straight and parallel again (Figure 6). In this zone, the vorticity shed from the body surface is been convected in the stream direction and diffused by viscosity. In addition, since vorticity is spreading continually, ultimately convection is more important than streamwise diffusion and that the streamwise gradient is small compared with that in the lateral plane. Thus the boundary-layer approximations are applicable asymptotically, irrespective of the Reynolds number of the flow based on the body size, although the distance downstream at which they are naturally applied depends on the circumstances, being greater for smaller Reynolds numbers and for bluff bodies.

A further effect accompanying the continual spreading of the wake is the tendency for frictional forces to make the velocity uniform. Thus, in addition to the boundary-layer approximations, it might be assumed that the departure from the free-stream velocity is small at positions sufficiently far downstream. Some analytical deductions about steady flow in this asymptotic region are described for the simple case on which only drag force acts.

The free-stream velocity has magnitude U and direction parallel to the z-axis say. The velocity and pressure in the irrotational flow outside the wake are approximately uniform (for z sufficiently large), and so the pressure is approximately uniform also in the wake. Moreover, $|U-u| << U$, and the component of acceleration in the z-direction is given approximately by

$U\frac{\partial u}{\partial z}$. The equation of motion far downstream in a steady wake therefore reduces to the linear equation:

$$U\frac{\partial u}{\partial z}=\nu\left(\frac{\partial^2 u}{\partial^2 x}+\frac{\partial^2 u}{\partial^2 y}\right) \tag{8}$$

Where ν is the cinematic viscosity of the fluid and coordinates *x* and *y* are the ones who form the plane perpendicular to the longitudinal axis z along the body wake.

Equation (8) is of the same form as the equation for conduction of heat transfer in the (x, y) plane in a solid (with *z/U* in (8) corresponding to time in the conduction equation), for which it is known that the solution in an infinite region tends to an asymptotic form independent, apart from a multiplicative factor, of the initial conditions. Finally, the asymptotic solution found is:

$$V_w=U-u=\frac{U_B Q}{4\pi\nu z}\exp\left[\frac{-U_B r^2}{4\nu z}\right] \tag{9}$$

Where the term *Q* is a constant determined by the conditions at some initial value *z,* is relative to the next relation:

$$Q=\frac{F_{DB}}{\rho U_B}=\frac{C_{DB}\pi R^2 U_B}{2} \tag{10}$$

This term can be obtained by the integration over the wake and directly it is directly related to the total drag force (F_{DB}) of the bubble. Comparing this expression with the one presented before relative to a Gaussian distribution, it can be seen that both of them have the same function form. It was then expected to find some experimental formula, obviously with the same form, with the objective to clarify whether experimental data would follow the theoretical model or not.

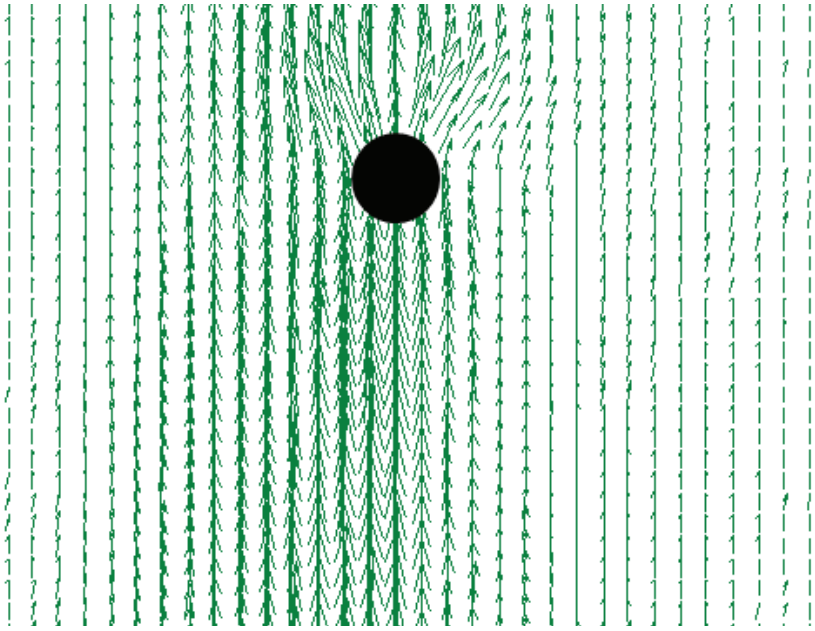

Figure 6. Bubble wake 35% glycerol Re = 67

6.2 Parameter V_{max} along axe z

By the time it was found a model in literature to compare with, a new process was started in order to find both V_{max} and s general equations. The first step was so to find V_{max}. As it has been told before, V_{max} is the term relative to the maximum speed velocity field value for each wake transversal section. This maximum value is reached for a radial coordinate $r = 0$. For each series of experiments, it was done a graphical comparison between the experimental data and the velocity distribution obtained through the application of the Oseen. Velocity values were normalized by dividing each of them by the bubble ascension velocity U_B . It was seen then than experimental data fitted well with theoretical model for points for a far wake near the bubble, whereas it did not follow the Oseen model for sections of the near wake (figure 6). After analysing all data for every series of experiments, it was found the next expression for the V_{max} *values*:

$$V_{max}(m/s) = U_B \exp[\alpha\sqrt{z}] \;\; ; \;\; \alpha = \frac{-5.26}{\sqrt[3]{\mathrm{Re}.Cd.d_B}} \qquad (11)$$

Parameter α has length unities [$m^{-0.5}$] in order to make the whole term non dimensional.

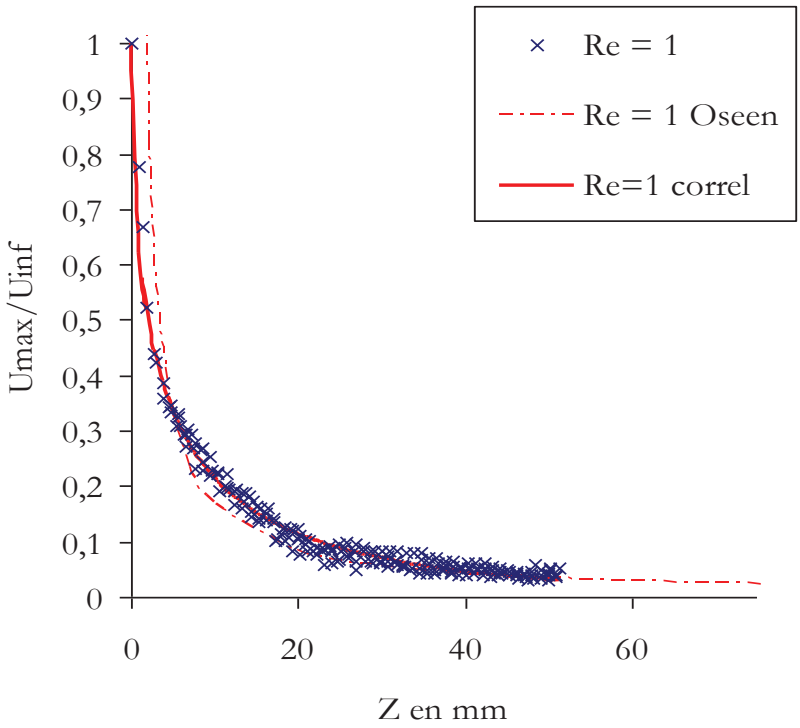

Figure 7. V_{max} distribution Re =1.

This figure shows three different series. The first one is related to experimental data, the second one is the graphical representation of the theoretical model proposed by Carl Wilhelm Oseen. Finally, the last series represents all values obtained by the general expression found empirically. It can be seen then that V_{max} depends on the rising bubble velocity, the diameter of the bubble and both Re and Cd non dimensional hydrodynamic parameters. After applying equation (11) with each series of experimental data, it was done a comparison between both values of V_{max} experimental and modelled. The error was always less than 7%.

6.3. Parameter s along axe z

The term relative to the standard deviation talks about the width of the Gaussian bell distribution along the axe z. A graphical representation was also carried out for every experimental series. It was found that the parameter *s* followed an increasing linear tendency. In this case, it was found a major dispersion in values with the growth of *z* values (Figure 7). After analyzing data, it was obtained the next expression:

$$s(mm) = 2\sqrt{\frac{\nu.z}{U_B}} + 4.d_B \qquad (12)$$

It can be seen from the previous expression that the standard deviation of the Gaussian Velocity distribution depends on the cinematic viscosity of the quiescent solution, the rising bubble velocity and the diameter of the bubble. This time, the error obtained between experimental values and modelled was higher than in the case of the parameter V_{max} (12% vs. 7%). The cause of this major error may be possibly explained by the major dispersion existent in the experimental data obtained.

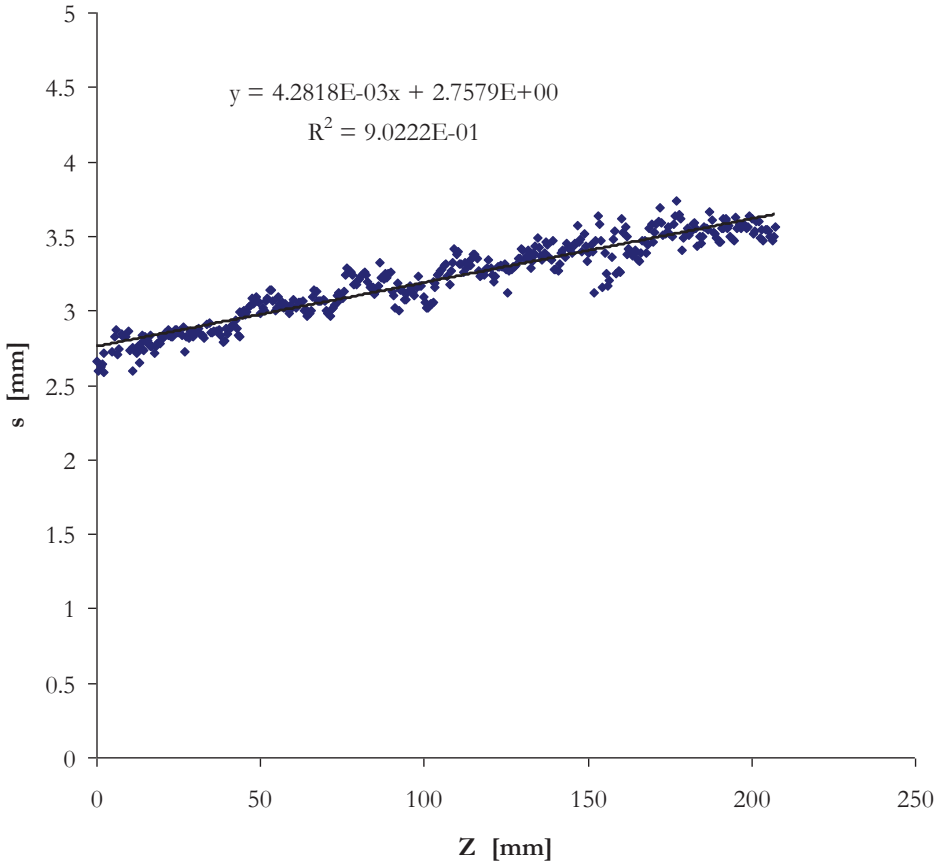

Figure 8. Parameter s distribution for Re =1.

6.4. Wake velocity field general equation

Once both V_{max} and s parameters were already calculated, it was possible to join them in order to find the general equation which described the wake velocity field:

$$V_W(r,z) = U_B.e^{\alpha.\sqrt{z}}.e^{-\frac{r^2}{\left(2.\sqrt{\frac{\nu z}{U_B}}+4.d_B\right)^2}}, \quad \alpha = \frac{-5.26}{\sqrt[3]{\mathrm{Re}.Cd.d_B}} \quad \alpha = \left[m^{-0.5}\right] \qquad (13)$$

It can be seen from this expression that the wake velocity field depends on different parameters. Some of them are relative to the bubble geometry (d_b), whereas the other ones are flow characteristics (Re, Cd, μ, ρ). This assembled expression carried an error which was never superior to 11%.

6.5. Validation of the model

After finally achieving a general expression, it was time to validate the model. With this purpose, it was done a parity diagram for each series of experiments, facing experimental values to the modelled ones. It was then seen that the found wake velocity field expression was successful, since quite all experimental data followed well the model, as it can be seen in figure 9. The error was never bigger than 6%.

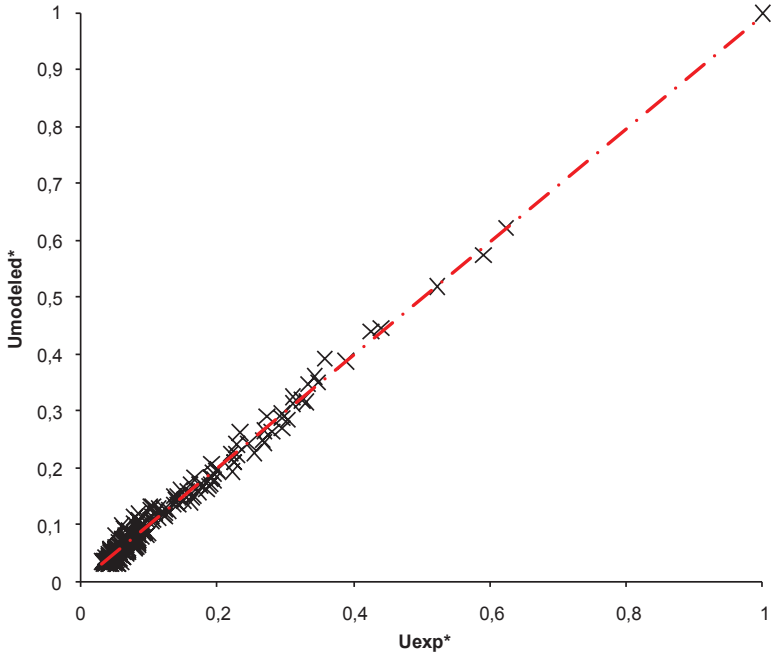

Figure 9. Parity diagram for Re =1

7. Wake velocity field modelling

7.1. Wake length

Once the general equation describing the bubbles wake velocity field was already calculated and validated, it was time to represent it by using the mathematical package Matlab. As this program allows us to represent 3D functions, it was possible to observe the spatial velocity distribution along the wake and to calculate the wake length for each series of the carried out experiments. In order to achieve this task, the chosen criterion was to look the velocity field distribution laterally, and find then the point in which the velocity value was zero. The length was measured in number of bubble diameters (see ***annexe 2*** Matlab figures). Finally, the following results were obtained:

Re	0.552	1.99	8.83	16.7	67	124.6
L_{wake} (d_b)	63	74	77	131	150	157

Afterwards, this length was graphically represented as a function of the Reynolds number of each series of experiments as it can be seen in figure 10.

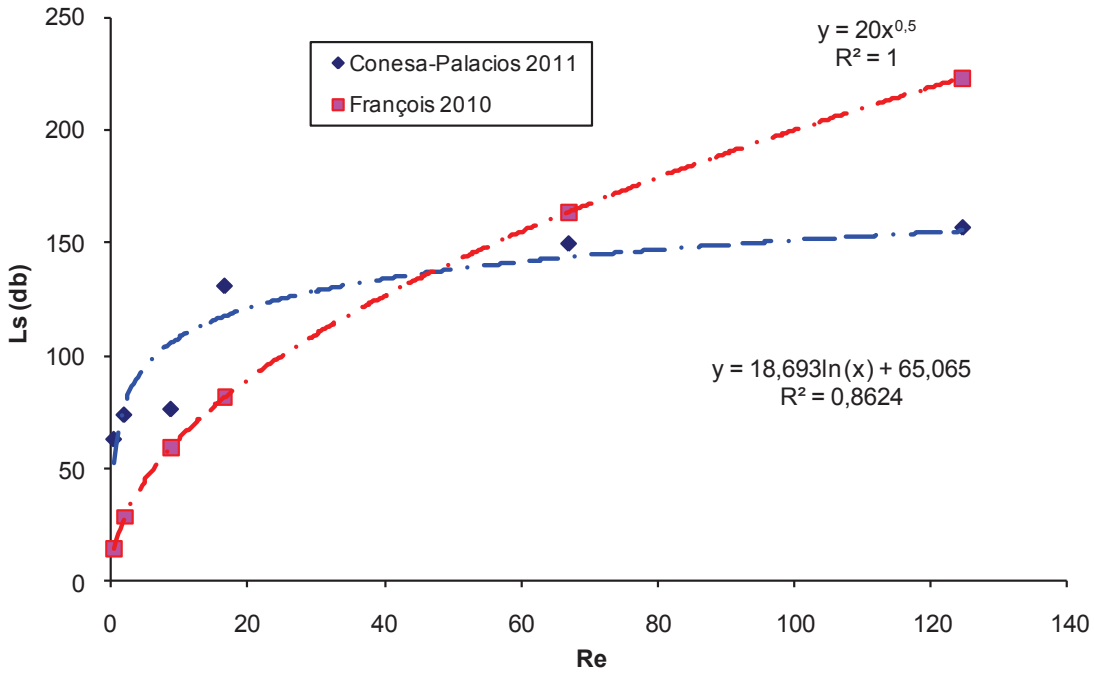

Figure 10. Wake length as a Reynolds number function

Figure 10 illustrates that the wake velocity field distribution follows an increasing logarithmic tendency. This figure also faces the wake length from the velocity field distribution (blue dotted series) against the oxygen concentration wake length (red dotted series). Oxygen concentration measurements were carried out by the engineer of studies Jessica François in 2010. It can be seen that the oxygen distribution increases its length more rapid with an increment of the Re number than the velocity distribution. Both wake lengths follow the next expressions (equations 14 and 15):

$$L_{velocity} = 18.693 Ln(\mathrm{Re}) + 65.065$$
$$L_{concentraton} = 20\sqrt{\mathrm{Re}} \qquad \text{(14) and (15)}$$

8. Perspectives

As it has been told before, gas-liquid reactors have nowadays an extremely important role in many industrial processes. Mass transfer phenomena quantification is directly linked to this type of reactors efficiency. On one hand, in this study it has been quantified the wake velocity field for a bubble wake under certain conditions (spherical bubbles in rectilinear ascension). To achieve this goal, all the experiments were carried out by using the PIV method (Particle Image Velocimetry). The laser plan was placed vertically in order to light the bubbles path. On the other hand, studies carried out by Jessica François to find the oxygen field concentration in the wake of bubbles used the PLIF method (Planar Light Induced Fluorescence). In his method, a laser plan is also used to illuminate the medium, which then fluoresces. The signal is captured by a detector and it is also related to medium properties in this case oxygen concentration. To find the oxygen concentration field, the laser plan was configured to illuminate the solution in a horizontal plane. In this way, it is no trivial to use all results from both studies in order to calculate the total flux of oxygen mass transfer, as they have been found by using clearly different experimental configurations. Now it is time to develop a deep analysis in order to face future calculations.

Figure 11 shows both velocity and oxygen field concentrations. As it can be clearly seen, velocity field is much wider than the concentration field, whereas the length of both wakes is nearly of the same order.

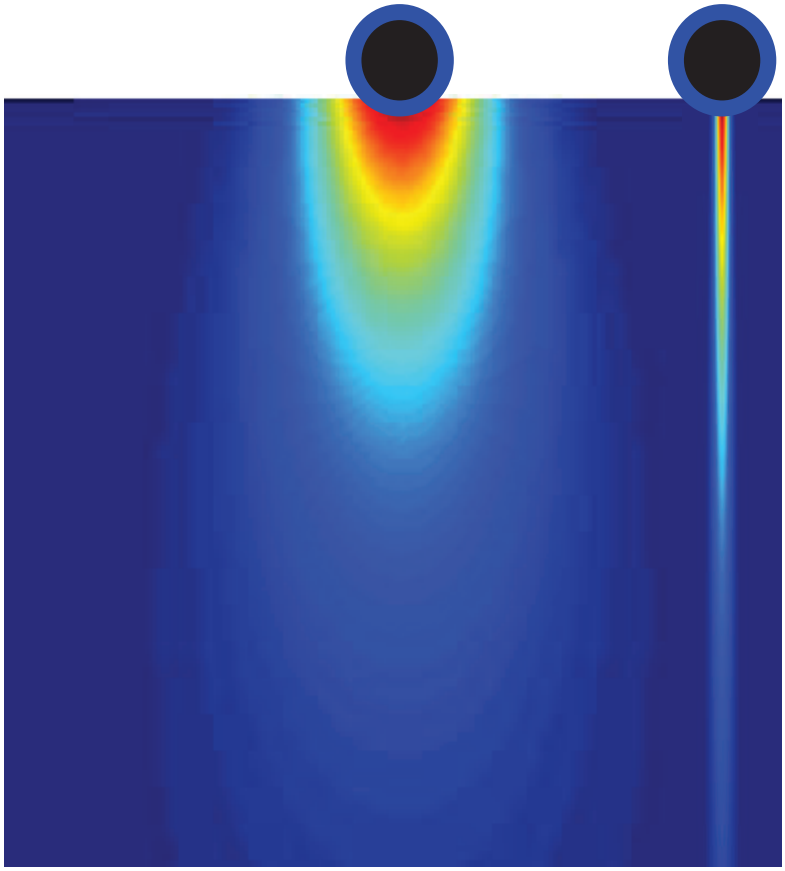

Figure 11. Velocity and oxygen concentration visual comparison

These figures were modelled by using the following theoretical expressions (equations 16 and 17):

$$V_W(r,z) = Ub.\frac{Cd.d.\mathrm{Re}}{32.z}e^{-\frac{r^2 U_B}{4Dz}}$$
$$C_{O_2}(r,z) = \frac{F_0}{4\pi Dz}e^{-\frac{r^2 U_B}{4Dz}} \qquad \text{(16) and (17)}$$

The expression of the wake velocity (16) is the Oseen equation developed in function of hydrodynamic parameters. The equation relative to the concentration field (17) follows also the Oseen equation structure.

9. Conclusions

Experimental and analytical results show clearly the efficiency of the PIV system as a non-intrusive technique, perfectly able to obtain precise results of the real fluid motion. Tracer particles task result much better than other traditional techniques since flow suffers no perturbation.

By the time all the experimental series had been carried out (using different glycerol and HV45 solutions), the following experimental data analysis showed clearly how the bubble wake velocity field followed a Gaussian distribution along the axis z. Then, it was done a calculation of both parameters V_{max} and s for every Gaussian velocity distribution for each section of every experimental series. The final step was then to find a general model which explained the velocity field as a function of different of various parameters. It was found that it depended on the bubble geometry (bubble diameter d_b, drag coefficient Cd), on different hydrodynamic parameters characteristics of the flow, such as the Reynolds number Re, the fluid density ρ and viscosity μ and finally on the bubble ascension velocity U_b. Later validation analysis through parity diagrams showed how the model fitted quite well with data acquired during the experiments, since the error was never worse than 6%.

Finally, both experimental results from the wake velocity field (2011) and oxygen concentration field (2010) gave us a chance to quantify the total flow of mass oxygen transfer around a bubble. Since the experimental procedure from both studies is clearly different, it is time to discuss and analyse results deeply enough to ensure that it is feasible to face further studies in order to achieve our final goal.

Notation

$C_D = \frac{4}{3}.g.\frac{d_B}{U_B^{\,2}}$	Drag coefficient, dimensionless
$\mathrm{Re} = \frac{U_B.D_B.\rho}{\mu}$	Reynolds number dimensionless
d_B	Bubble diameter, mm
d_p	Tracer particle diameter, mm
D_i	Colloidal diffusion coefficient, $m^2.s^{-1}$
F_{Db}	Bubble drag force, Newtons
g	gravity, $m.s^{-2}$
k	Boltzmann's constant
L_{wake}	Wake length, d_B
M_i	Molar mass, $g.mol^{-1}$
r	radial coordinate, mm
r_p	Tracer particles radios, mm
s	Standard deviation from Gaussian Distribution, mm
t	time, s
T	Temperature, K
u	Flow velocity, $m.s^{-1}$
U_b	Bubble velocity ascension, $m.s^{-1}$
$V_{max}(z)$	Maximum velocity value for every wake section, $m.s^{-1}$
V_s	Sedimentation Velocity of a tracer particle, $m.s^{-1}$
V_w	Wake velocity, $m.s^{-1}$
V_x	Flow horizontal Velocity for a certain point, $m.s^{-1}$
V_y	Flow vertical Velocity for a certain point, $m.s^{-1}$
x	distance, mm
x_i	molar fraction
y_i	distance, mm
z	distance, mm

Greek letters

λ_a	absorption wavelength, nm
σ_p	Random displacement tracer particle, microns.s^{-1}
μ	Dynamic viscosity, Pa.s
ν	Kinematic viscosity, $m^2.s^{-1}$
ρ	density, kgm^{-3}

Subscripts

∂D_B	Bubble contour
∂D_G	Geometric contour
B	Bubble
P	Particle
W	Wake

References

F. White, *Fluid Mechanics*, McGraw-Hill Companies 5th Edition

J. K. Batchelor, *An introduction to Fluid Dynamics*, Cambridge University Press

R.H. Perry, Perry's C hemical Engineers Handbook, McGraw-Hill Companies

Antoine Whilelmus Gerardus de Bries, *Path and wake of a rising bubble*, University of Twenty 2001

Jian Zhang & Liang-Shih Fan, *On the rise velocity of an interactive Bubble in liquids*, Department of Engineering Mechanics, Tsinghua University Beijing China & Department of Chemical Engineering, The Ohio State University USA

M.C. Ruzicka, *On bubbles rising in line*, Institute of Chemical Process Fundamentals, Czech Academy of Sciences, October 1998

Fan Wenyuan, MA Youguang, Li Xiaolei, and Li Huaizhi, *Study on the flow field around two parallel moving bubbles and interaction between bubbles rising in CMC solutions by PIV*, Chinese Journal of Chemical Engineering, 2009

J.D. Bugg, G. A. Sad, The velocity field around a Taylor bubble rising in a stagnant viscous fluid: numerical and experimental results, International Journal of Multiphase Flow, 2002

R.C. Chen, I. S. Chou, Wake structure of a single bubble rising in a two dimensional column, Experimental Thermal and Fluid Science, 1998

Annexe 1

Experimental Set - up photos

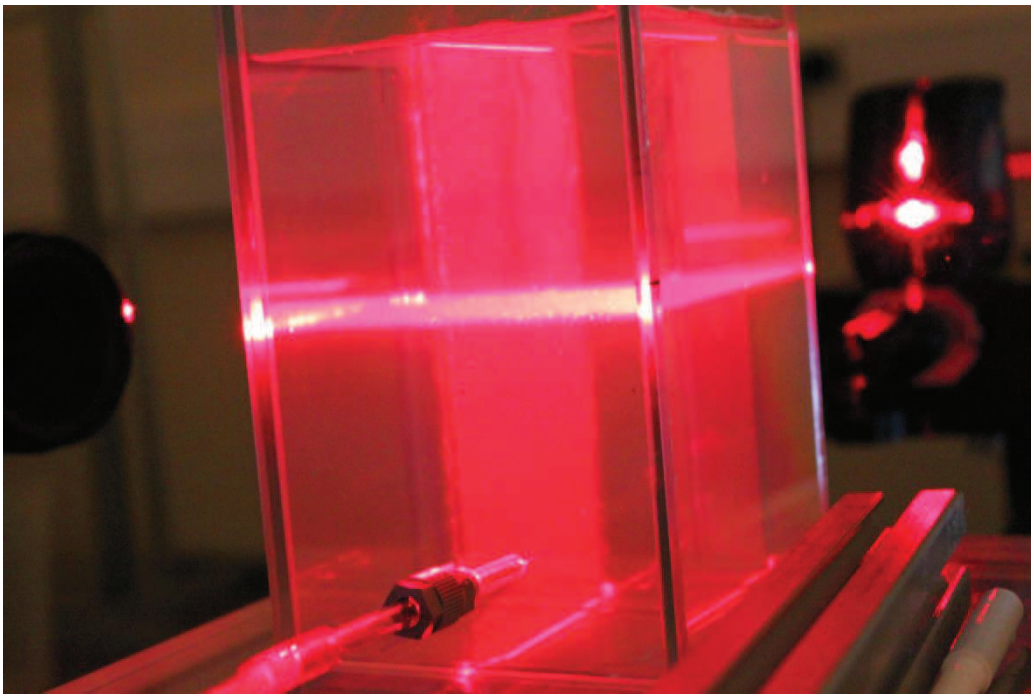

Figure 1. Laser plan adjustment over capillary

Figure 2. Experimental room

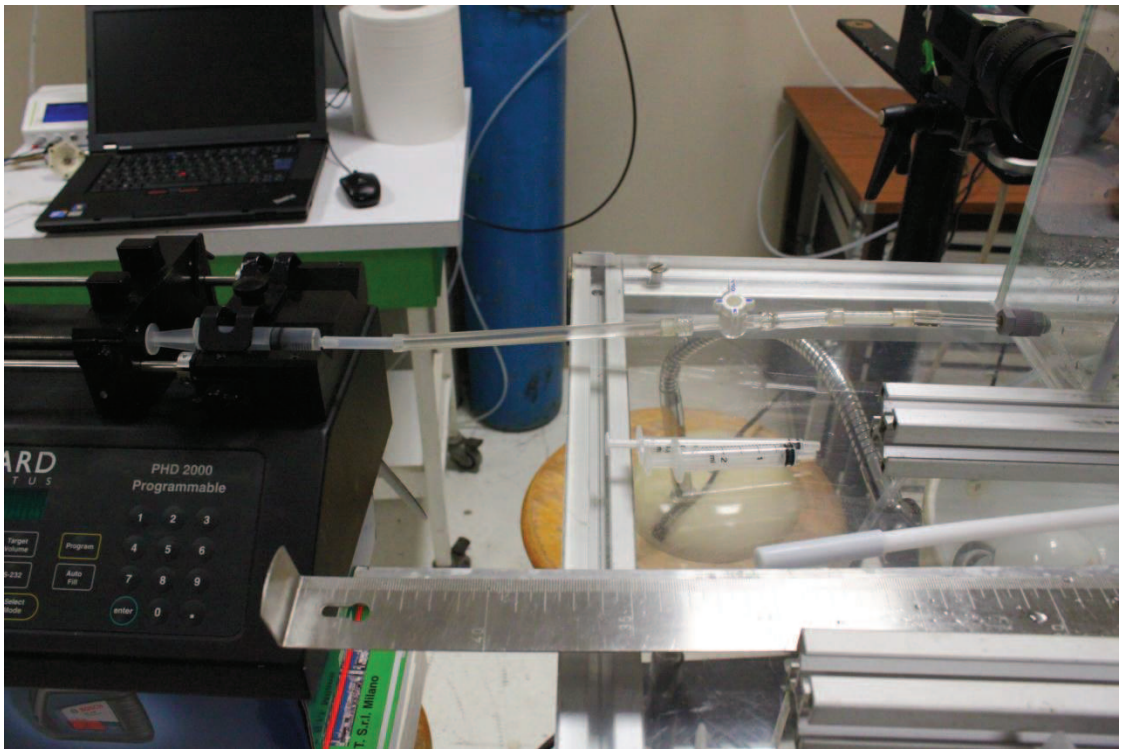

Figure 3. Air injection circuit system

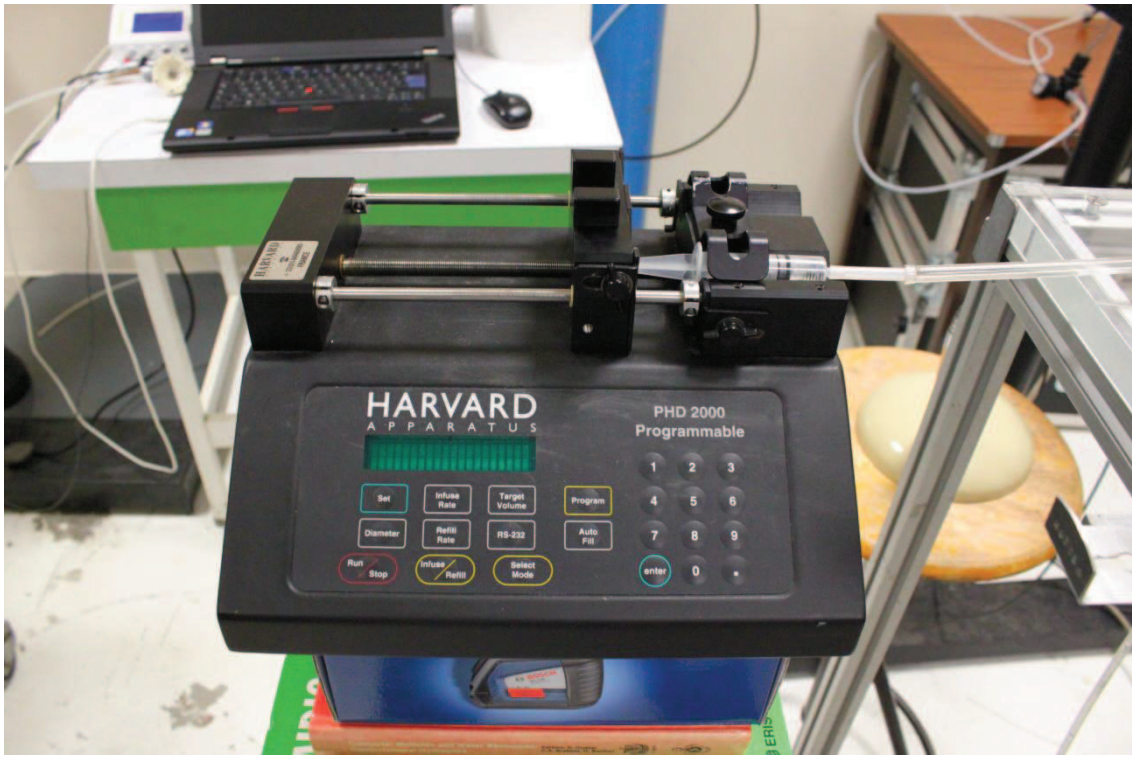

Figure 4. Programmable syringe pump

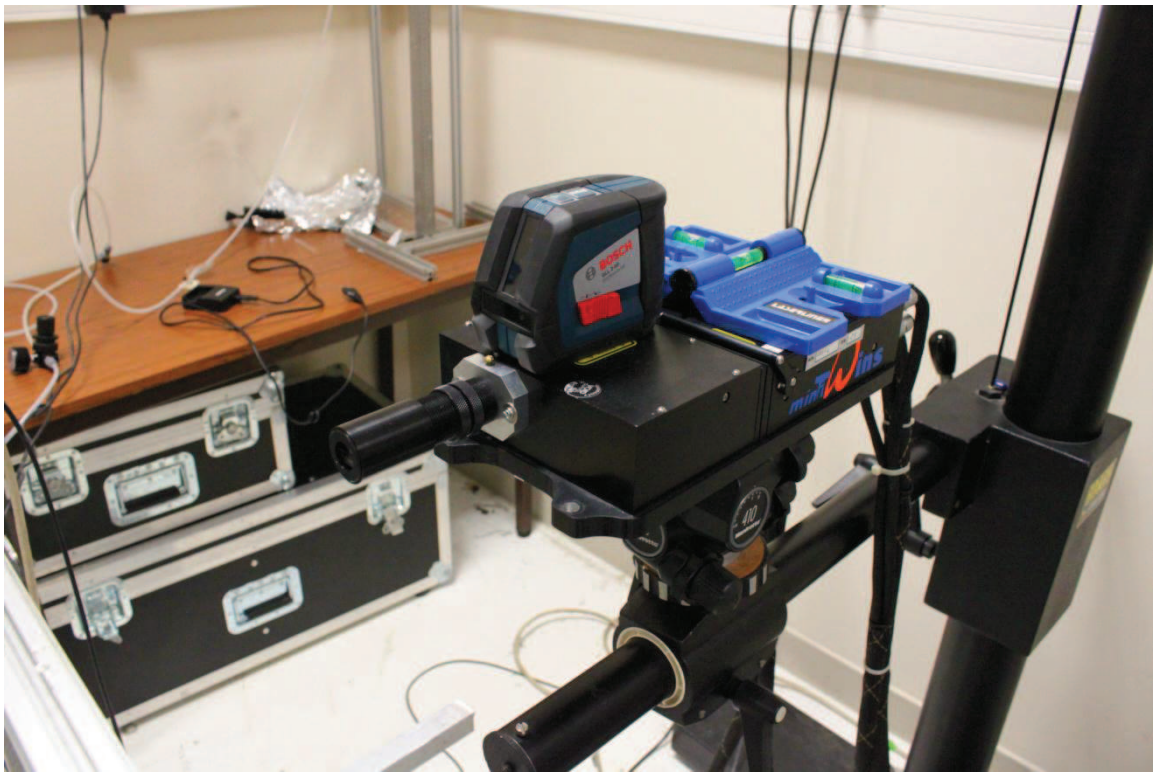

Figure 5. Laser

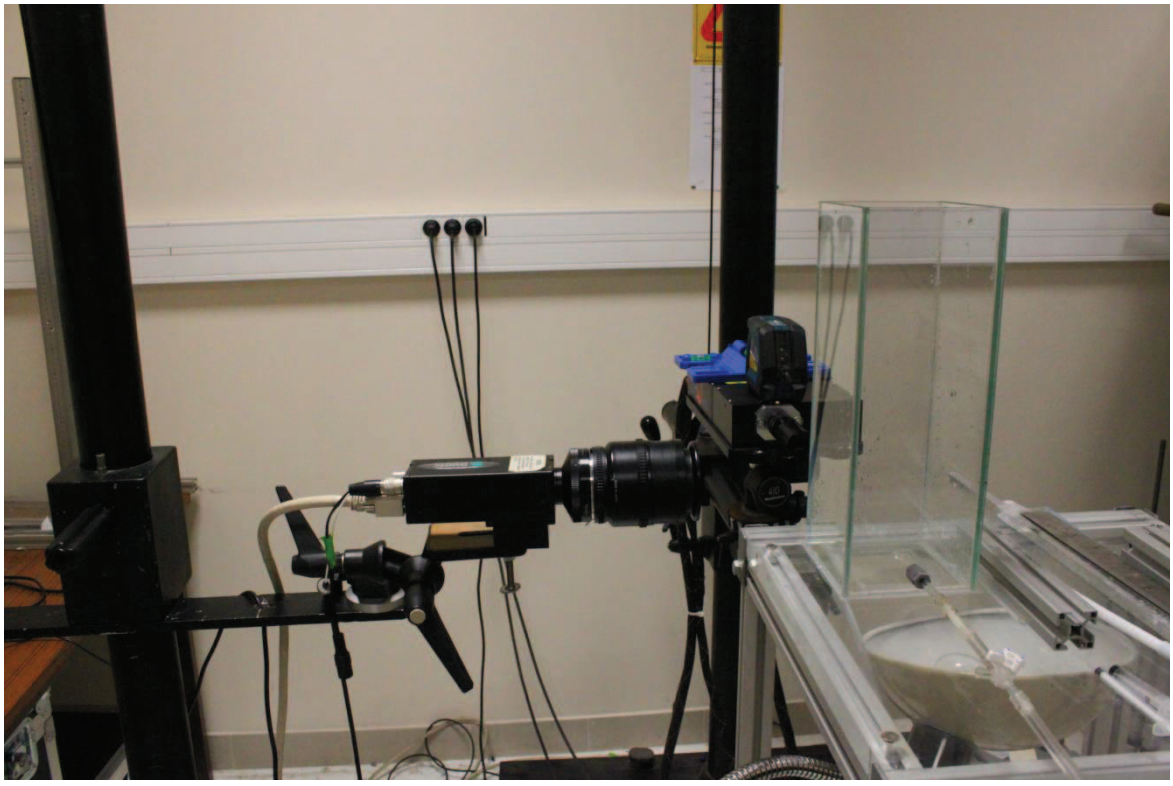

Figure 6. High speed camera, laser, prism container of the solution, capillary and laser

Annexe 2

Re = 0.5, U_b = 0.037 m/s, d_b = 3 mm, μ= 0.2 Pa.s, Cd = 32.035

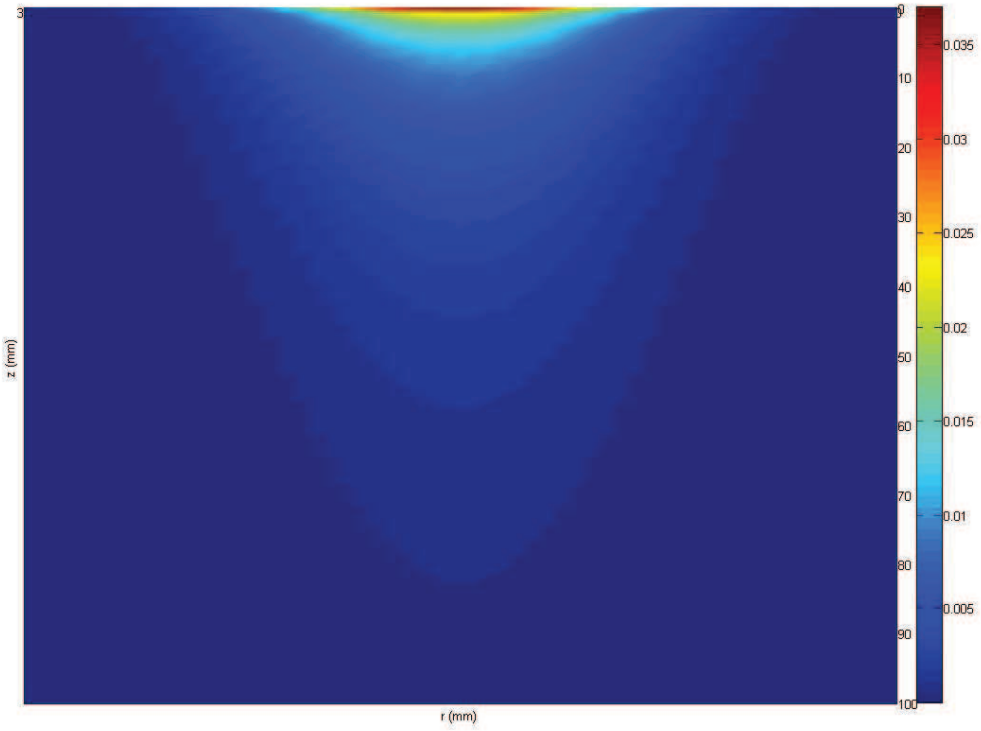

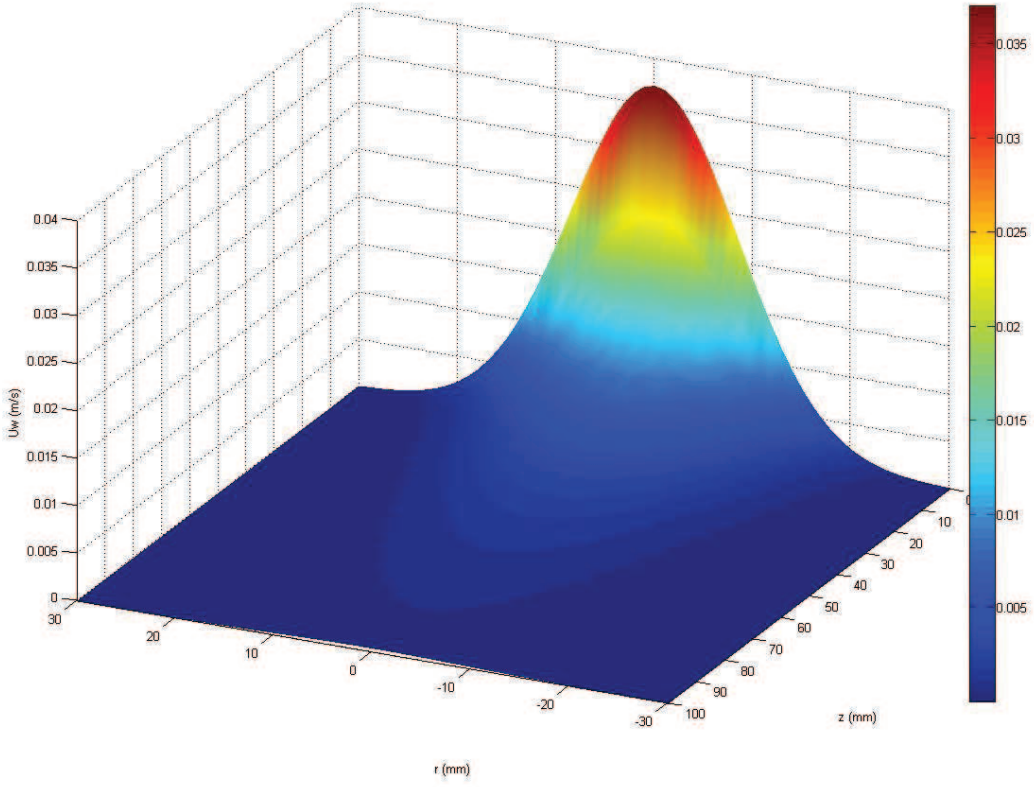

Re = 1.99, U_b = 0.069 m/s, d_b = 2.9 mm, μ= 0.1 Pa.s, Cd = 10.888

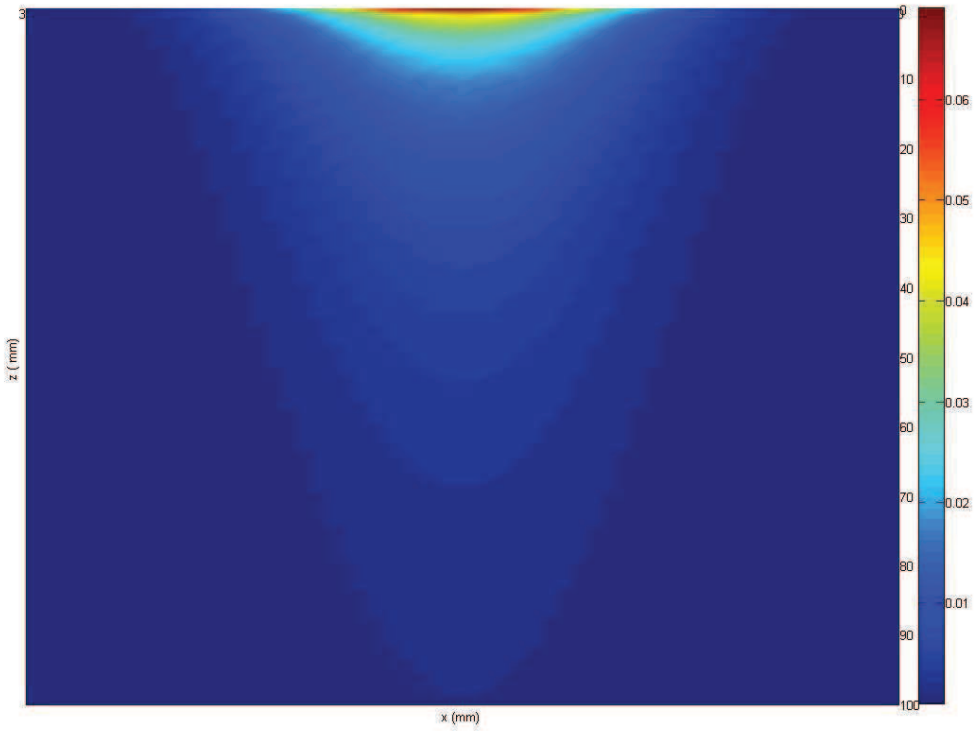

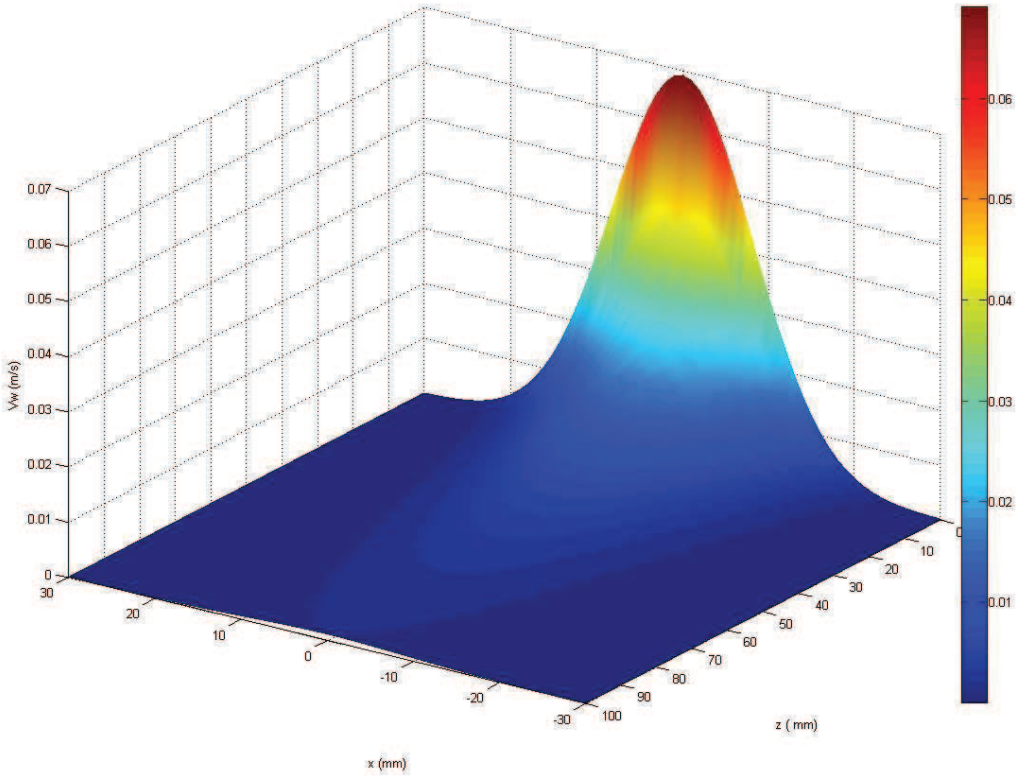

Re = 8.83, U_b = 0.147 m/s, d_b = 3 mm, μ= 0.05 Pa.s, Cd = 3.581

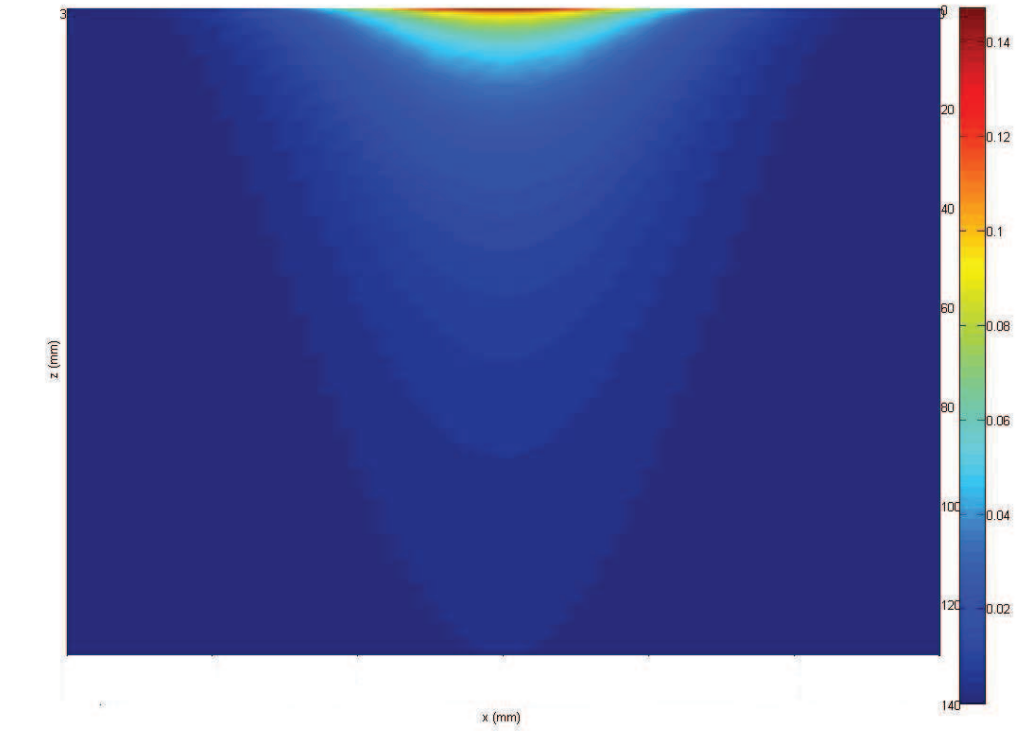

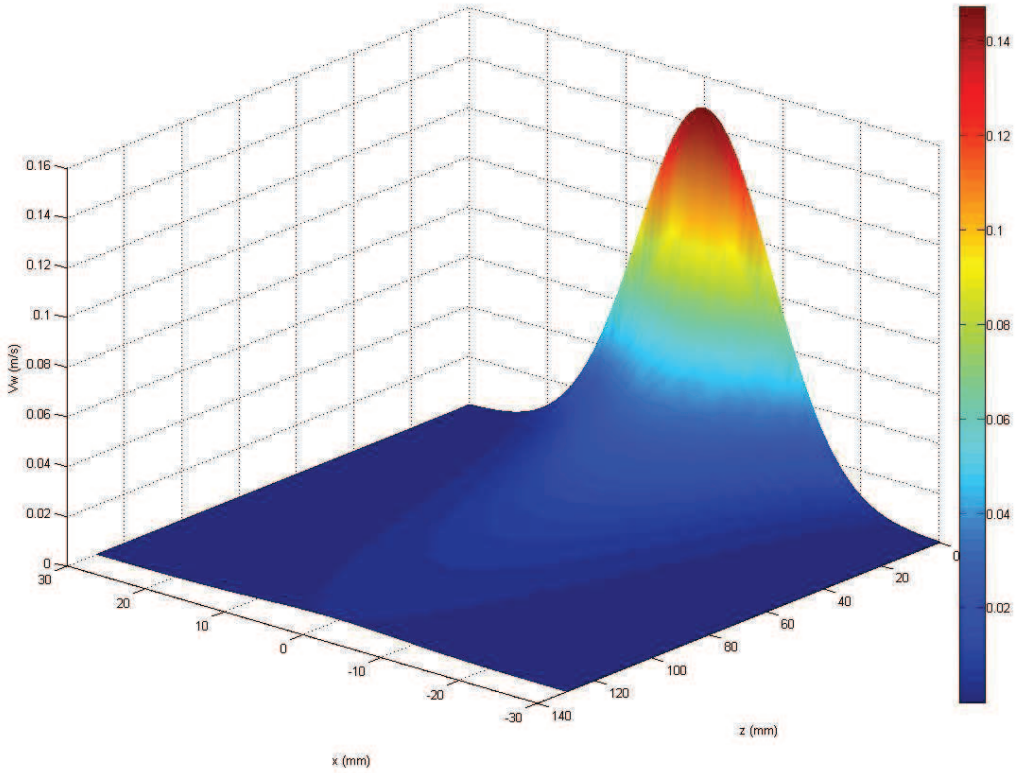

Re = 16.7 U_b = 0.105 m/s, d_b = 0.8 mm, μ= 0.005 Pa.s, Cd = 2.217

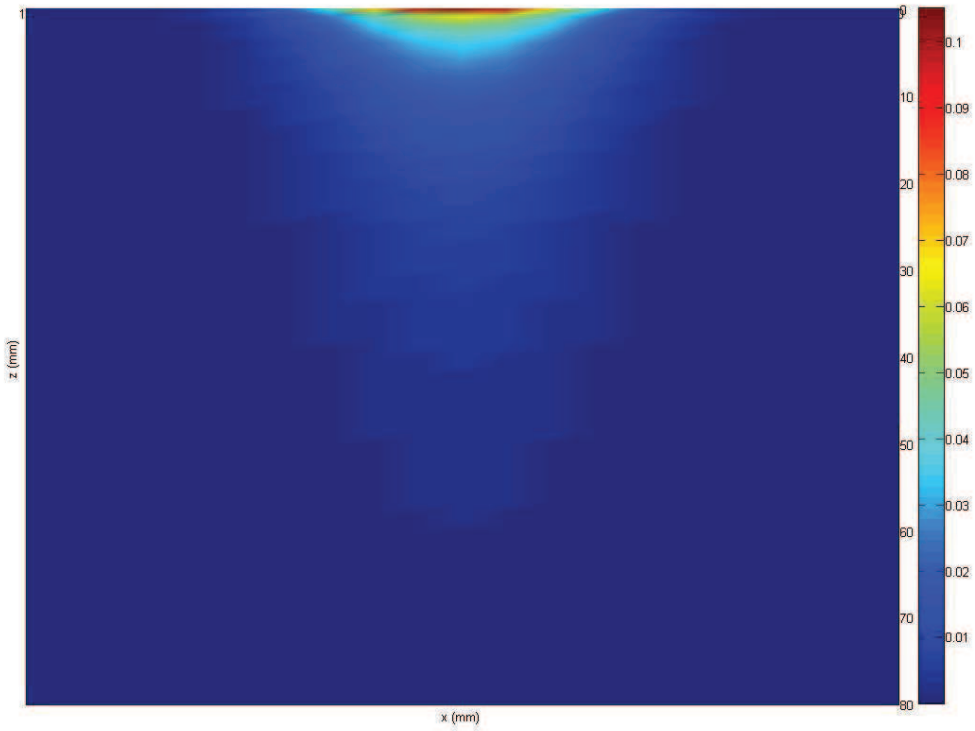

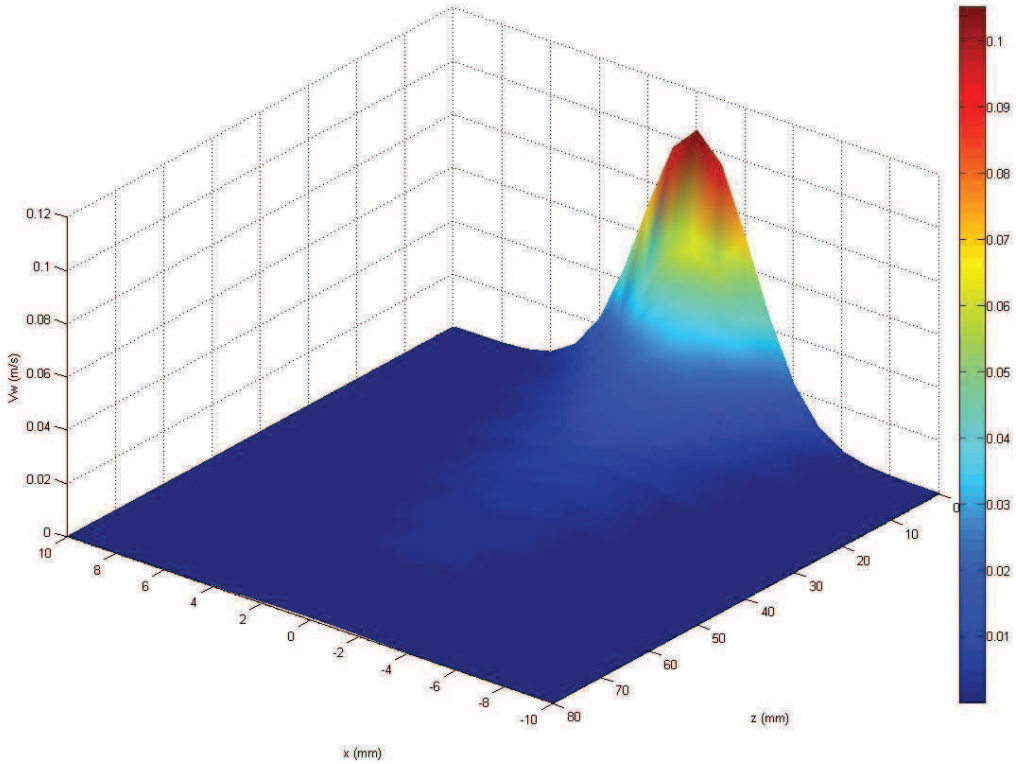

Re = 67, U_b = 0.209 m/s, d_b = 0.8 mm, μ= 0.0025 Pa.s, Cd = 0.689

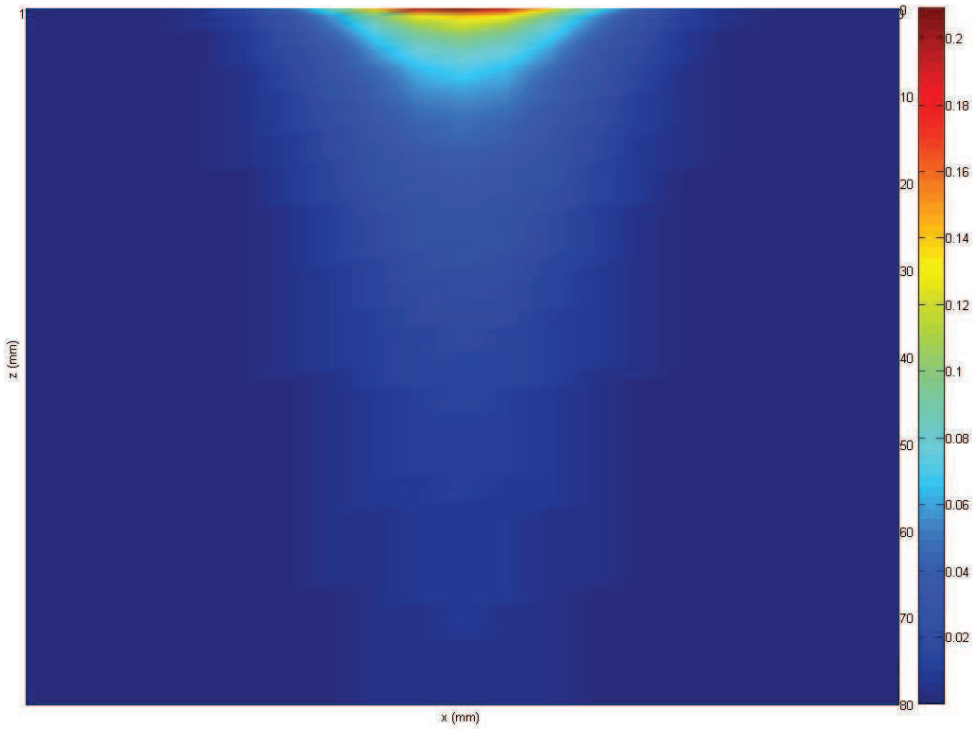

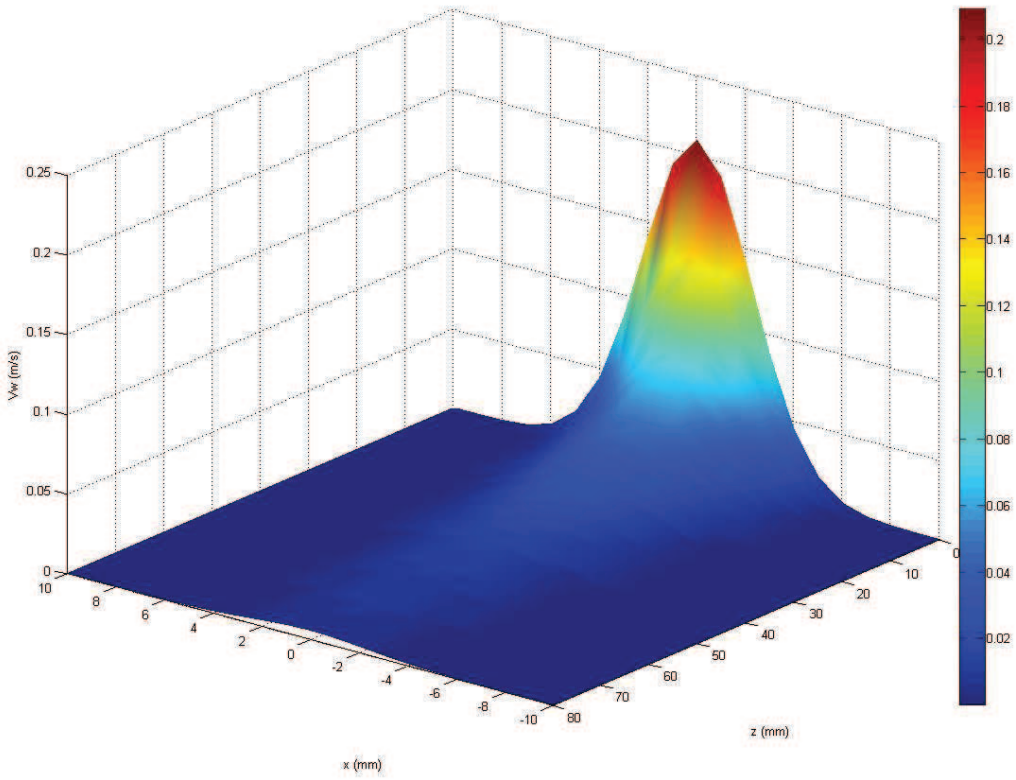

Re = 124, U_b = 0.267 m/s, d_b = 0.79 mm, μ= 0.00128 Pa., Cd = 0.385